

# Gas Dynamics in the Luminous Merger NGC 6240

L.J.Tacconi, R.Genzel, M.Tecza and J.F.Gallimore<sup>1</sup>

Max-Planck Institut für extraterrestrische Physik (MPE), D-85748 Garching, Germany

D.Downes

Institut de Radio Astronomie Millimétrique (IRAM), 38406 St. Martin d'Hères, France

and

N.Z. Scoville

California Institute of Technology, 105-24, Pasadena, CA 91125

Received \_\_\_\_\_; accepted \_\_\_\_\_

Submitted to ApJ: 26 January 1999; Accepted: 28 April 1999

---

<sup>1</sup>present address: National Radio Astronomy Observatory, Charlottesville, VA 22903

## ABSTRACT

We report  $0''.5 \times 0''.9$  resolution, interferometric observations of the 1.3 mm CO J=2→1 line in the infrared luminous galactic merger NGC 6240<sup>2</sup>. About half of the CO flux is concentrated in a rotating but highly turbulent, thick disk structure centered between the two radio and near-infrared nuclei. A number of gas features connect this  $\sim 500$  pc diameter central disk to larger scales. Throughout this region the molecular gas has local velocity widths which exceed  $300 \text{ km s}^{-1}$  FWHM and even reach FWZP line widths of  $1000 \text{ km s}^{-1}$  in a number of directions. The mass of the central gas concentration constitutes a significant fraction of the dynamical mass,  $M_{gas}(R \leq 470 \text{ pc}) \sim 2\text{-}4 \times 10^9 M_{\odot} \sim 0.3\text{-}0.7 M_{dyn}$ . We conclude that NGC 6240 is in an earlier merging stage than the prototypical ultraluminous galaxy, Arp 220. The interstellar gas in NGC 6240 is in the process of settling between the two progenitor stellar nuclei, is dissipating rapidly and will likely form a central thin disk. In the next merger stage, NGC 6240 may well experience a major starburst like that observed in Arp 220.

---

<sup>2</sup>Based on observations carried out with the IRAM Plateau de Bure Interferometer. IRAM is supported by INSU/CNRS (France), MPG (Germany) and IGN (Spain).

## 1. Introduction

In the last two decades it has become clear that collisions and mergers of galaxies are important processes that trigger spectacular starburst and nuclear activity, and that play a critical role in the evolution of galaxies (e.g. Sanders and Mirabel 1996, Genzel, Lutz and Tacconi 1998). Hierarchical merging of smaller sub-units into bigger ones was probably a key process in the formation of galaxies. It is, therefore, of obvious importance to study and understand in detail some prototypical examples of nearby merger systems.

The galaxy NGC 6240 (D=97 Mpc for  $H_o = 75 \text{ km s}^{-1} \text{ Mpc}^{-1}$ ,  $1'' = 470 \text{ pc}$ ) belongs to the class of [ultra]-luminous infrared galaxies ([U]LIRGs) whose radiation output largely emerges in the infrared band ( $L_{bol}(\text{NGC 6240}) \sim L_{IR} = L_{8-1000\mu m} = 6 \times 10^{11} L_{\odot}$ , Sanders et al. 1988, Thronson et al. 1990, Sanders and Mirabel 1996). The main characteristics of NGC 6240 are:

- Its optical/near-infrared/radio morphology is dominated by two compact sources (hereafter referred to as ‘nuclei’) at a separation of  $\sim 1''.6(750 \text{ pc})$ , surrounded by a highly disturbed stellar disk structure along P.A. =  $25^{\circ}$  E of N (Fried and Schulz 1983, Thronson et al. 1990, Colbert et al. 1994). The large de-reddened K-band luminosities<sup>3</sup> of these two main emission peaks ( $L(K) \sim 2 \times 10^9 L_{\odot}$  for the south and  $\sim 1 \times 10^9 L_{\odot}$  for the north nucleus) show that they must be massive:  $\geq 1 \times 10^9 M_{\odot}$  and  $\geq 5 \times 10^8 M_{\odot}$  for the south and north nuclei, respectively. They are more than just bright star forming regions and are very plausibly individual galaxy nuclei.

NGC 6240, thus, is very probably a system of colliding/merging galaxies that we are viewing prior to the final merging of the two progenitor nuclei into one.

---

<sup>3</sup> $L(K) \simeq (\nu L_{\nu})_{2.2\mu m} \times (\Delta\lambda/\lambda)_{K\text{-band}}$ , where the fractional width of the K-band is  $(\Delta\lambda/\lambda)_{K\text{-band}} \sim 0.23$ .

- The infrared to radio continuum spectral energy distribution and the mid-/far-infrared line emission indicates that a large fraction of the bolometric luminosity of NGC 6240 comes from a recent but aging starburst (Colbert et al. 1994, Lutz et al. 1996, Genzel et al. 1998). In addition, 5-10 keV X-ray continuum emission, 6.7 keV Fe  $K\alpha$  emission ( $L_x/L_{IR} \sim 10^{-2}$ , Kii et al. 1997, Nakagawa et al. 1999) and fairly strong  $26\mu\text{m}$  [OIV] mid-IR line emission (Lutz et al. 1996, Genzel et al. 1998, Egami et al. 1999) all strongly suggest that an AGN is present and probably significantly contributes to  $L_{bol}$ .
- Ionized gas with velocity widths of up to  $1000 \text{ km s}^{-1}$  is observed in optical emission lines, such as  $H\alpha$  (Heckman, Armus and Miley 1987, 1990; Armus, Heckman and Miley 1990, Bland-Hawthorn et al. 1991). Heckman, Armus and Miley (1987) and Armus, Heckman and Miley (1990) interpret the dynamics and hour-glass shaped morphology of the  $H\alpha$  emission (along P.A. =  $110^\circ$ , perpendicular to the large scale disk) in terms of a powerful superwind triggered by the nuclear activity and supernova explosions. The ratio of kinetic energy input by the wind to bolometric luminosity is about 1.5% (Heckman et al. 1990).
- NGC 6240 has the most powerful infrared  $H_2$  line emission so far found in a galaxy (Joseph et al. 1984;  $L(H_2) \sim 2 \times 10^9 L_\odot$ ; Egami et al. 1999). The  $2\mu\text{m}$   $H_2$   $v=1 \rightarrow 0$  S(1) emission is centered between the two radio/infrared nuclei (Herbst et al. 1990; van der Werf et al. 1993; Tecza et al. 1999) and probably is excited in shocks due to the galaxy collision (van der Werf et al. 1993). Intense millimeter CO rotational line emission indicates that  $\sim 10^{10} M_\odot$  of dense molecular interstellar gas is concentrated in the central kiloparsec (Wang, Scoville and Sanders 1991, Solomon, Downes and Radford 1997, Bryant and Scoville 1999). The large amount of molecular gas near the nuclei implies large equivalent column densities of dust ( $N(H_2) \geq 2 \times 10^{23} \text{ cm}^{-2}$  or  $A_V \geq 200$ ). It also suggests that gas constitutes a significant fraction of the dynamical

mass.

- The late type stars in the region of the double nucleus have a very large velocity dispersion,  $\sigma = 350 \pm 20 \text{ km s}^{-1}$  in  $1''.5$  to  $2''.2$  diameter apertures (Lester and Gaffney 1994, Doyon et al. 1994). This dispersion is much larger than that observed in gas-rich, disk galaxies, and is at the upper end of what is observed for massive elliptical galaxies (Doyon et al. 1994, Whitmore, McElroy and Tonry 1985, Bender et al. 1994). The ratio of dynamical mass to dereddened total K-band stellar luminosity for the N6240 system is  $M(\text{dyn})/L(\text{K}) = 4.5$  for a K-band screen extinction of  $A(\text{K})=0.5\text{--}0.7$  (Genzel et al. 1998). For a single stellar population this ratio is fit by an age  $\sim 1$  Gyr, assuming that the dynamical mass is due to the stars dominating the near-infrared light, that star formation is constant with time, and that the initial mass function is Scalo (1986) down to a lower mass cutoff of  $0.2 M_{\odot}$ . This age is inconsistent with the equivalent width of the CO bandhead absorption. The latter implies that the K-band light is dominated by massive red supergiants of age 10–30 million years (Lester et al. 1988, Tecza et al. 1999). The discrepancy can only be resolved if the main carrier of the dynamical mass does not contribute to the near-infrared light.

To investigate the spatial distribution and dynamics of the neutral gas component in this prototypical merger system we have carried out high resolution imaging spectroscopy of the CO  $J = 2 \rightarrow 1$  line at 1.3 mm with the IRAM mm-interferometer on the Plateau de Bure. Our new data shed light on the merger dynamics and evolution.

## 2. Observations and Data Reduction

We have mapped the  $^{12}\text{CO } J=2 \rightarrow 1$  line in NGC 6240 with the IRAM millimeter interferometer on the Plateau de Bure, France (Guilloteau et al. 1992). The data were

obtained between January and February 1998. The array consisted of 5 15- meter antennas positioned in 3 different configurations providing 30 baselines ranging from 32 to 408 meters. Since the CO line emission is  $\sim 1000 \text{ km s}^{-1}$  wide, we observed with two different local oscillator setups centered  $\pm 250 \text{ km s}^{-1}$  from the assumed systemic velocity of  $7339 \text{ km s}^{-1}$ , providing an equivalent bandwidth of 970 MHz ( $1300 \text{ km s}^{-1}$ ). We observed NGC 6240 for  $\sim 6$  hours in each configuration and LO setting for a total of about 36 hours of integration time (18 hours integration per velocity channel). Each antenna was equipped with dual-frequency SIS receivers enabling us to observe the HCN  $J=1\rightarrow 0$  line at 86.5 GHz simultaneously with the CO  $J=2\rightarrow 1$  line. The SIS mixers have receiver temperatures of 60–80 K, and are used in single-sideband mode at 3 mm and double-sideband mode at 1 mm. The system temperatures, corrected to outside the atmosphere, are 120 K and 400 K respectively. The phases and amplitudes were calibrated by observing 1655+077 every half hour, and the bandpass was calibrated by observations of 3C273. The absolute flux scale is based on a flux of 14 Jy for 3C273 at 225 GHz. Fluxes of strong sources are determined through careful monitoring with both the interferometer and the IRAM 30-meter telescope on Pico Veleta, Spain. The data are of excellent quality; based on the monitoring measurements, the accuracy of the flux scale is expected to be better than 30%. The phase noise on the longest baselines was  $20^\circ\text{--}30^\circ$  rms at 1 mm. Spectral resolution of 2.5 MHz ( $\sim 3.3 \text{ km s}^{-1}$  at 1 mm and  $6.5 \text{ km s}^{-1}$  at 3 mm) was provided by 6 autocorrelator spectrometers for each of the two LO frequency settings, covering the total 970 MHz bandwidth. The data were calibrated using the CLIC software package written at IRAM. We then made and CLEANed uniformly weighted channel maps using software from the GILDAS package. To increase the sensitivity we smoothed the data spectrally to a resolution of  $20 \text{ km s}^{-1}$  before mapping. The CLEANed CO maps were reconvolved with a  $0''.9 \times 0''.5$  FWHM beam (P.A.= $26^\circ$ ), and the HCN  $1\rightarrow 0$  maps were reconvolved with a  $2''.5 \times 1''.4$  FWHM beam (P.A.= $29^\circ$ ). The rms noise (per channel) after CLEANing was  $\sim 4$

mJy beam<sup>-1</sup> for the CO 2→1 data and 0.8 mJy beam<sup>-1</sup> for the HCN 1→0 maps.

We also observed NGC 6240 using the six element Multi-Element Radio-Linked Interferometer (MERLIN) based at Jodrell Bank (Wilkinson 1992). The observing frequency was 5 GHz with a bandwidth of 15 MHz. We observed two tracks: one horizon-limited track on 7 Dec 1997 and a shorter track on 9 Dec 1997, for a total on-source integration time of roughly 11 hours. Phase calibration solutions were determined by interleaved scans of the phase calibrator B1648+015 with a duty cycle of six minutes source to one minute calibrator. The flux scale was set by the daily scan of 3C 286 bootstrapped to the phase calibrator. Initial calibration and editing employed the Jodrell Bank DPROG software package. We used standard fast Fourier transform imaging software in the AIPS software package provided by NRAO <sup>4</sup> Two iterations of self-calibration improved the phase calibration solutions for the source. The resolution of the naturally-weighted synthetic map is  $94 \times 50$  milliarcseconds into P.A.  $21^\circ$ , and the image sensitivity is 0.1 mJy beam<sup>-1</sup>.

### 3. Results

The basic results of our CO 2→1 interferometric observations of NGC 6240 are shown in Figures 1 through 6. Figure 1 shows selected spectra and a logarithmic image of the integrated CO line emission. Figure 2 shows uniformly weighted maps in  $\Delta v = 40$  km s<sup>-1</sup> resolution velocity channels. Figure 3 displays a 228 GHz continuum map made from the upper sideband, and a superposition of red- ( $v \geq 350$  km s<sup>-1</sup>) and blue-shifted ( $v \leq -350$  km s<sup>-1</sup>) line wing emission. Figure 4 gives the second moment map of the CO emission (intensity weighted measure of dispersion around the mean), and position-velocity

---

<sup>4</sup>The National Radio Astronomy Observatory is operated by Associated Universities, Inc., under contract with the National Science Foundation.

diagrams of data and an appropriate disk model. Figure 5 displays selected spectra in the central concentration along with those of the model disk. Figure 6 shows an overlay of integrated and red-/blue-shifted CO maps on top of the 8 GHz radio continuum map of Colbert et al. (1994) and the 5 GHz MERLIN map. Table 1 summarizes the measured fluxes and source parameters. We next summarize our basic findings.

### 3.1. Spatial distribution of the gas

Most of the CO 2→1 emission in NGC 6240 comes from the central 3'' radius region ( $\sim 1.5$  kpc). We detect a total of 1220 Jy km s<sup>-1</sup> of CO flux from NGC 6240. It is difficult to say how much of the single dish flux we detect, since published single dish spectra span insufficient bandwidth to include enough continuum for proper subtraction. For instance, the spectra of Combes et al. (1991) and Casoli et al. (1992) span only 660 km s<sup>-1</sup> and they quote an integrated line strength of  $\sim 800$  Jy km s<sup>-1</sup>. For comparison, we measure  $\sim 1000$  Jy km s<sup>-1</sup> over the same bandpass. The discrepancy probably owes to the baseline subtraction in the single dish spectra. Since the line covers the entire single dish band, baseline subtraction would remove both continuum and an indeterminate amount of line flux. Solomon et al. (1997) measure a CO 1→0 integrated intensity of 69 K km s<sup>-1</sup> in a 22'' aperture in NGC 6240. This converts to a 2→1 flux of 1000 Jy km s<sup>-1</sup>, assuming that <sup>12</sup>CO 2→1/1→0 ratio is 0.8 (Casoli et al. 1992). It is thus likely that we are recovering most of the CO line emission in our interferometric map.

Of the total source line flux, 528 Jy km s<sup>-1</sup>, or 43% is concentrated in a  $\sim 1''$  diameter thick disk-like structure located in between the two radio/infrared nuclei (Figure 6). Such a distribution was strongly suggested in the lower resolution CO map of Bryant and Scoville (1999). The aspect ratio of the integrated CO distribution in Figure 1 is 1:2 (EW:NS), slightly larger than the aspect ratio expected from the inclination of the large scale disk



(1:3 for  $i \sim 70^\circ - 75^\circ$ , Fried and Schulz 1983). The two nuclei are located approximately at either end of this central gas disk. This is best seen in Figure 6 (middle) which compares the 5 GHz MERLIN map with the integrated CO emission shown on a linear intensity scale. The centroid of the integrated CO emission is somewhat closer to ( $0''.6$  NNE of) the brighter, southern nucleus.

Only the two main nuclei are detected by the MERLIN observations (Figure 6b); the extended radio structure in the VLA maps of Colbert et al. (1994; Figure 6a) is mostly resolved below the sensitivity of the MERLIN images. The extended radio structure surrounding the southern nucleus matches well the sidelobe pattern of the aperture synthesis beam and is probably an artifact of the imaging and calibration process. There is no compact radio (or infrared) continuum source at or near the position of the CO peak, neither on the  $0''.15$  resolution 8 GHz map of Colbert et al., nor on the  $0''.08 \times 0''.035$  5 GHz MERLIN map. This and the fact that the total radio flux density from the two nuclei falls right on the radio-far-infrared correlation for star forming galaxies if one takes the total far-infrared flux from the IRAS data (Colbert et al. 1994) strongly suggests *that there is no strong luminosity source hidden at the center of the CO emission*. However, there is a bridge of extended 8 GHz emission connecting the southern and northern nuclei and approximately following the general outline of the CO emission.

The orientation of the long axis of the CO disk (P.A.  $\sim 10^\circ - 20^\circ$ , Figure 1) is about the same as that of the large scale galactic disk of NGC 6240 but somewhat tipped away from the kinematic major axis as derived in this paper (see section 3.2). There are several distinct gas features in the integrated and channel maps surrounding this central structure and extending to spatial scales of  $3'' - 4''$ . These features can be best identified in the channel maps (see below). A second, smaller CO peak ( $220 \text{ Jy km s}^{-1}$  of the total flux of  $1220 \text{ Jy km s}^{-1}$ ) is located  $4'' - 5''$  NNE of the CO maximum. The second peak (the ‘northern clump’)

was first seen in the 7'' CO 1→0 interferometry map of Wang, Scoville and Sanders (1991). It does not correlate with any feature in the radio continuum, infrared or optical maps.

The HCN 1→0 emission is confined to the central  $\sim 3''$  radius region of the CO peak. We detect a total of 12 Jy km s<sup>-1</sup> from this region. The profiles and widths of the HCN lines are very similar to those seen in CO when the two data sets are smoothed to the  $2''.5 \times 1''.4$  resolution of the HCN map. This is an indication that the emission from both species arises from the same dense gas throughout the region of the CO peak. Since the CO data are of much higher spatial resolution the rest of the paper is devoted to the CO results alone.

### 3.2. Kinematics of the gas

The neutral gas in NGC 6240 is highly disturbed, with unusually large velocity widths almost everywhere in the central 3''. Typical line widths ( $0''.5 \times 0''.9$  beam) are FWHM 300–400 km s<sup>-1</sup> and FWZP 700–1000 km s<sup>-1</sup>. In the region  $\sim 0''.5 - 1''.5$  north of the peak even the  $\pm 540$  km s<sup>-1</sup> <sup>5</sup> range covered by our two LO settings was not sufficient to include all of the line emission (Figure 1). In this region there are red wings extending to at least +600 km s<sup>-1</sup>. A study of the spectra in Figure 1 and the channel maps in Figure 2 reveals that there are several distinct kinematic components.

In the central disk the centroids/peaks of the highly blueshifted emission ( $-250$  to  $-480$  km s<sup>-1</sup>) and of the highly redshifted emission ( $300-550$  km s<sup>-1</sup>) are separated by  $0''.75$  along P.A.=40° (Figure 3 and Figure 6, bottom). The average position of the blue- and red-shifted emission centroids is coincident with the peak of the  $2\mu\text{m}$  vibrationally excited H<sub>2</sub> emission (Tecza et al. 1999) and is  $\sim 0''.15$  S of the CO integrated flux peak. The most

---

<sup>5</sup> All velocities in the text are relative to  $v_{hel} = 7340$  km s<sup>-1</sup>

likely interpretation of this large velocity gradient is rotation of the central disk with a line of nodes along a P.A. of  $30^\circ - 45^\circ$ . However, the line profiles in the central structure all are singly peaked, rather than the double-horned profiles characteristic of a rotating disk. To wipe out the classical double-horn there are probably two effects at work: (1) the gas motions could have a very large random component and (2), the rotation curve of the disk could be steeply rising from the center outwards. These effects could combine most effectively if most of the disk emission comes from the lower velocity central part of the disk. In addition, radiative transport effects in an optically thick disk may further decrease the contrast between the optically thicker, high velocity edges and the thinner lower velocity parts of the emission profile. We investigate possible models in more detail below. It is very unlikely that the velocity gradient is caused by a bipolar outflow. The molecular gas mass in the central disk significantly exceeds  $10^9 M_\odot$  (see section 4). The kinetic energy of the outflow thus would be  $\geq 10^{57.5}$  ergs. The dynamical lifetime of the present central CO concentration would then be  $\leq 10^6$  years and the mechanical energy deposition rate would be  $\geq 10^{10.5} L_\odot \geq 0.05 L_{bol}$ . This deposition rate exceeds the mechanical luminosity of the superwind by a factor of 3 or more. These energy and time scale considerations make an outflow scenario very improbable. In addition, it is then unclear where the origin of the outflow is, since there is no radio source at the center of the CO peak. In this scenario it is not obvious why the two radio nuclei are located at either end of the disk.

There are a number of separate gas features connecting the central 500 pc to the larger scale disk (indicated as letters A through E on Figure 1). These features are also present in the  $2\mu\text{m}$   $\text{H}_2$  maps of Herbst et al. (1990), van der Werf et al. (1993) and Tecza et al. (1999). The two most prominent of these (A, B) emanate from the southern edge of the disk and arch to the SW and SE on either side of the southern nucleus (Figures 1 and 2). Both features can be easily recognized on the integrated line maps as well as in the channel maps (Figures 1 and 2), largely because they have very broad lines (Figure 1). As in the central

region the broad lines all along the lengths of these features are in fact their most prominent characteristic. Systematic velocity gradients along the features are comparatively small. The gas in feature C leads from the center to the SE and is mainly blueshifted ( $-250$  to  $0$   $\text{km s}^{-1}$ ), with a possible connection to a lower velocity long filament stretching toward the NE. Features D and E consist of redshifted gas ( $100$  to  $500$   $\text{km s}^{-1}$ ) with very wide lines. They connect the northern edge of the central concentration to the NNE and NNW, with a possible bridge to the northern clump at  $\sim 200$   $\text{km s}^{-1}$ . Taken together features A+B and D+E appear to form a ‘butterfly’ pattern emanating from the nuclear concentration to the north and south, straddling around the two infrared/radio nuclei.

NGC 6240 is highly unusual because of these large chaotic velocities. None of the several other ULIRGs/mergers studied so far with high resolution mm- interferometry have these characteristics (e.g. Yun and Scoville 1995, Bryant and Scoville 1997, Scoville et al. 1997, Downes and Solomon 1998, Sakamoto et al. 1999). It is difficult to interpret the kinematics and gas distribution as a simple, orbital motion or uniform flow. The most likely interpretation of the enormous line widths is that they largely represent line of sight projections in a complex, highly chaotic gas flow. This system has many streamers with a wide range of angular momenta and orbital parameters. In addition one would expect that the large velocity widths cause shocks and dissipation. Dissipation of the cloud kinetic energy through shocks naturally explains the luminous infrared molecular hydrogen emission; recall that NGC 6240 is the most luminous  $\text{H}_2$  line source currently known (Rigopoulou et al. 1999, section 5.1). The fact that these motions still exist in the central regions of NGC 6240 argues for this system being in a relatively early phase of merging before the chaotic motions have been dissipated.

### 3.3. Rotating disk model of the central disk

In order to quantify the dynamical properties of the central CO disk we fit the data by an axisymmetric turbulent, rotating disk (see Tacconi et al. 1994). Recognizing that the gas distribution and kinematics are, in detail, more complicated than a simple axisymmetric model, the main disk parameters were tuned interactively to fit the principal characteristics of the data and to represent the axisymmetrically averaged gas properties. Table 2 lists the parameters (gas density distribution, rotation curve and local turbulent velocity dispersion) of our best disk model. The position-velocity diagrams for the model disk and the observed CO 2→1 emission along P.A. = 40° (the dynamical major axis of the central disk) are shown in Figure 4. The observed and model line profiles are compared in Figure 5. The key ingredients of this model are a bright central gas concentration at radii of up to 0".5, a rising rotation curve to a maximum of  $280 \pm 40 \text{ km s}^{-1}$  at  $R \sim 0".75$  (for an assumed inclination of  $70^\circ - 75^\circ$ ) and a large turbulent velocity width of FWHM  $300 \pm 50 \text{ km s}^{-1}$ . The inferred model rotation curve as a function of radius is plotted in Figure 7. The average ratio of rotation velocity in the central disk to the one dimensional velocity dispersion ( $\sigma \sim 0.43 \text{ FWHM}$ ) is  $\langle v_{rot} \rangle / \sigma \sim 2$ , with a range of 1 to 3. This indicates that the central molecular disk is highly turbulent. This, in turn, implies that the disk is geometrically thick. These dynamics and the mass density (see below) are similar to those of stars in cores of elliptical galaxies (Bender et al. 1994). In fact the model requires a FWHM  $z$ -thickness of about 0".7 (330 pc) in order to match the profiles in the SE and NW corners of the central concentration (Figure 5). However, even with this large scale height the model profiles fit the data poorly S, SW and SE of the peak. This probably indicates that separate kinematical systems, perhaps related to the streamers A through C that appear to merge here into the central disk, are present. It is impossible for any axisymmetric kinematic model to reproduce all of the complicated kinematic and spatial structures observed in a violent merger event such as that of NGC 6240.

The large local line widths and relatively small, large scale velocity gradients suggest that radiative transport effects through the disk may play a role. Following Downes and Solomon (1998) we have computed models based on the disk code of Dutrey, Guilloteau and Simon (1994) with parameters appropriate for NGC 6240. The code, which was modified by Downes and Solomon, includes non-LTE radiative transport effects to account for finite opacity. For the relatively small optical depths that best fit the CO emission characteristics of NGC 6240 (section 4 see below) the kinematic parameters derived from the radiative transfer model are very similar to those listed in Table 2.

Since the gas dynamics are midway between a rotationally supported, cold rotating disk and a dispersionally supported, hot system it is appropriate to analyze the gas dynamics in terms of the observed velocity dispersion as well. Figure 4 shows the second moment map,  $\sigma_v$ ,<sup>6</sup> of the CO 2→1 emission. Taking  $\sqrt{2}\sigma_v$  as a measure of the equivalent circular velocity, the rotation curve inferred from this map is in excellent agreement with the results of the rotating disk model in Table 2 (see Figure 7). The dispersion increases from the CO flux peak to a maximum of 210 km s<sup>-1</sup> (equivalent circular velocity of 300 km s<sup>-1</sup>) in an oval ring at projected radius 0".5 – 1" and then decreases slowly at larger radii. *We thus conclude from modeling the gas dynamics that there is a prominent concentration of mass centered on the CO flux peak (between the radio/infrared nuclei) which is extended over about 1".* In a separate paper (Tecza et al. 1999) we show from sub-arcsecond resolution near-infrared field imaging spectroscopy that the stellar dynamics in the center of NGC 6240 also supports this conclusion. Tecza et al. show that the stellar velocity dispersion peaks between the two nuclei, even after they account for the rotation of the stars in the individual nuclei.

While the axisymmetric disk model provides a satisfactory overall fit to the large scale structures observed in the p-v diagram (Figure 4), it deviates significantly from the data

---

<sup>6</sup> $\sigma_v = [\int (v^2 - \langle v \rangle^2) I_{CO}(v) dv] / [\int I_{CO}(v) dv]$

in the central, low velocity emission (Figure 5). Compared to the model, the observed line profile is asymmetric and the peak emission is blue-shifted by a few tens of  $\text{km s}^{-1}$  with respect to the velocity centroid of the outer, high velocity emission (Figure 4). This discrepancy is mirrored in the channel maps, which show that the peak emission is centered  $\sim 0''.15$  north) of the line connecting the peaks in the blue and red wings. The central disk is therefore not strictly axisymmetric. There may also be additional spatial and kinematic substructure of the gas very near the center and at the individual IR/radio nuclei which will require higher resolution.

### 3.4. 1.3 mm continuum map

The spatial distributions of 1.315 mm (228 GHz) continuum and CO 2 $\rightarrow$ 1 line emission are clearly different (Figure 3). The continuum emission is dominated by the slightly resolved southern nucleus (4.5 mJy,  $19\sigma$  detection), with a second weaker component (1.4 mJy,  $6\sigma$  detection) on the northern nucleus. There is no obvious continuum peak on the central CO concentration other than perhaps a shoulder NNE of the south nucleus. If the non-thermal 8 GHz flux densities of the two nuclei (31 and 14 mJy, Colbert et al. 1994) are extrapolated with the radio spectral index (between  $-0.6$  and  $-0.7$ ), one would expect 2.9–4.2 mJy and 1.3–1.9 mJy at 1.315 mm for the southern and northern nuclei, respectively. These fluxes densities are consistent with our measurements. The 1.3 mm emission from the two nuclei, thus, is largely non-thermal synchrotron emission. Any continuum source associated with the central CO concentration would have to be weaker than 3 mJy within  $R \leq 1''$ . We discuss the lack of  $\lambda = 1.3$  mm continuum emission from the central CO concentration below.

## 4. Gas Dominates the Central Mass Concentration

Our CO J=2→1 maps show a prominent concentration of molecular gas centered in between the two radio/near-infrared nuclei. The gas concentration is also the center of rotation and marks the maximum of velocity dispersion in both the stars and the gas. The observational evidence points to the CO peak coinciding with a mass concentration between the nuclei. In this section we show quantitatively that this mass concentration is largely due to the (self-gravitating) interstellar gas itself.

### 4.1. Comparison of sizes of CO emission and mass concentration

If the CO flux accurately traces the distribution of molecular gas mass, one would qualitatively expect that the radial distributions of the circular velocity<sup>7</sup> and of the square root of the ratio of CO flux within radius R divided by that radius are similar. That is, the kinetic energy (rotational plus random) should vary with radius as the ratio of the interior CO flux to the radius. This is in fact the case (Figure 7, left).

### 4.2. Gas mass estimates

There are several approaches to estimating the gas mass quantitatively. A lower limit to the gas mass can be obtained by assuming that the CO J=2→1 emission is optically thin. From excitation calculations with gas temperatures between 50–100 K, local molecular hydrogen volume densities between  $10^3$ – $10^4$  cm<sup>-3</sup>, a CO to H<sub>2</sub> fractional abundance ratio

---

<sup>7</sup> the circular velocity  $v_c(R)$  and the mass enclosed within R,  $M(R)$ , are related through  $GM(R) = v_c^2(R)R$ . This relationship holds exactly for a spherical mass distribution, and approximately also for a disk-like axisymmetric distribution (Binney and Tremaine 1987).



of  $8 \times 10^{-5}$  and a 38% by mass contribution to the gas mass by helium we find for the optically thin case

$$M_{gas}(\text{CO thin}) = 2 \times 10^6 L_{CO2 \rightarrow 1} [\text{Jy km s}^{-1}] D_{97Mpc}^2 [\text{M}_\odot] \quad (1)$$

approximately independent of temperature. Taking the observed flux in the central  $R \leq 1''$  ( $528 \text{ Jy km s}^{-1}$ ), the equivalent optically thin gas mass is  $1.1 \times 10^9 \text{ M}_\odot$ . However, neither the observed peak brightness temperature (21 K), nor observed  $^{12}\text{CO}$  and  $^{13}\text{CO}$  line ratios can be matched in this optically thin limit. Casoli et al. (1992) find that the  $^{12}\text{CO}$   $2 \rightarrow 1/1 \rightarrow 0$  brightness temperature line ratio (corrected for beam and source size effects) is  $\sim 0.8$  and the  $\frac{^{12}\text{CO}1 \rightarrow 0}{^{13}\text{CO}1 \rightarrow 0}$  line ratio is  $\sim 44 \pm 17$ . Using a large velocity gradient excitation model we find that a match to the  $^{12}\text{CO}$   $2 \rightarrow 1$  brightness temperature, the  $\frac{^{12}\text{CO}2 \rightarrow 1}{^{12}\text{CO}1 \rightarrow 0}$  line ratio, and the  $\frac{^{12}\text{CO}1 \rightarrow 0}{^{13}\text{CO}1 \rightarrow 0}$  line ratio can be obtained with molecular hydrogen column densities from  $1 - 4 \times 10^{19} \text{ cm}^{-2}/(\text{km s}^{-1})$ , which yields a  $^{12}\text{CO}$   $2 \rightarrow 1$  line with  $\tau \sim 1 - 4$ . For this case the gas mass is

$$M_{gas}(\text{radiative transport}) = 4.2 \times 10^6 L_{CO2 \rightarrow 1} (\text{Jy km s}^{-1}) D_{97Mpc}^2 [\text{M}_\odot] \quad (2)$$

resulting in a mass of  $2.2 \times 10^9 \text{ M}_\odot$  within the central  $R=1''$ . For self-gravitating, virialized molecular clouds at kinetic temperature  $T$  and average molecular hydrogen density  $\langle n(H_2) \rangle$  the gas mass (again 38% helium) is also proportional to the integrated CO  $2 \rightarrow 1$  flux in the optically thick limit (due to the mass dependence of the overall line width; see Dickman et al. 1986, Genzel 1992) via

$$M_{gas}(\text{GMCs}) = 3.1 \times 10^7 L_{CO2 \rightarrow 1} (\text{Jy km s}^{-1}) D_{97Mpc}^2 (X/X_G) [\text{M}_\odot] \quad (3)$$

Here the conversion factor  $X$  between  $H_2$  column density and CO intensity ( $I_{CO}(\text{K km s}^{-1})$ ) is given in units of the Galactic value appropriate for  $T \sim 10 \text{ K}$ ,  $\langle n(H_2) \rangle \sim 200 \text{ cm}^{-3}$ , and  $X_G = 2.3 \times 10^{20} [\text{cm}^{-2}/(\text{K km s}^{-1})]$  (e.g. Bloemen et al. 1989). Assuming that the gas kinetic temperature in NGC 6240 is close to the average dust temperature,  $T \approx T_{dust} \sim 52 \text{ K}$

(Solomon et al. 1997, Draine 1990) and that the average  $H_2$  volume density is  $\sim 200 \text{ cm}^{-3}$  we find

$$(X/X_G)_{NGC6240} = \left(\frac{10K}{T}\right) \left(\frac{\langle n(H_2) \rangle}{200\text{cm}^{-3}}\right)^{0.5} \sim 0.2 \quad (4)$$

We estimate mean  $H_2$  densities of a few hundred  $H_2 \text{ cm}^{-3}$  from the CO source size and the total gas mass (Table 1). Based on the argument that in very luminous infrared galaxies, such as NGC 6240, the molecular gas is not clumped into self-gravitating clouds but is distributed in an intercloud medium with total gas masses less than the dynamical mass (Downes et al. 1993), Solomon et al. (1997) and Downes and Solomon (1998) also infer  $X/X_G \sim 0.2$  but find variations of factors of 3–4 from galaxy to galaxy. With these assumptions equations 3 and 4 yield  $M_{gas}(\text{GMCs}) \sim 3 \times 10^9 M_\odot$  for the central  $R \leq 1''$ .

Draine (1990) has estimated the total dust mass and gas mass (gas-to-dust mass ratio of 100) in NGC 6240 from dust emission models for the overall far- infrared/submillimeter spectral energy distribution. Depending on the number and temperature of dust components contributing to the emission he finds total gas masses ranging between  $6 - 70 \times 10^9 M_\odot$ . Assuming that the spatial distribution of the far-infrared emission is similar to that of the CO 2→1 emission, about half of that mass, or  $3 - 35 \times 10^9 M_\odot$ , is expected to be in the central  $R \leq 1''$  region.

Finally, the optically thin 1.3 mm continuum emission can be used to derive an upper limit to the gas mass (for  $M_{gas}/M_{dust} = 100$ )

$$M_{gas}(1.3 \text{ mm}) = 3.8 \times 10^8 S_{228}[\text{mJy}] D_{97Mpc}^2 \nu^{-4} (0.0014/\kappa_{228}) (52K/T_{dust}) [M_\odot] \quad (5)$$

Here  $S_{228}$  is the continuum flux density at frequency  $\nu = 228 \text{ GHz}$ , and  $\kappa_{228}$  is the dust absorption coefficient at 228 GHz. Since the 1.3 mm continuum emission is almost certainly optically thin it has the potential for being the most unambiguous method of determining the gas mass in the central disk. However both  $\kappa_{228}$  and the gas-to-dust mass ratio are very poorly known. This severely increases the 0 of masses derived in this manner. The value

for  $\kappa_{228} = 0.0014 \text{ cm}^2 \text{ g}^{-1}$  used in equation 5 is taken from Draine and Lee (1984) and  $\kappa$  scales with frequency as  $\nu^2$ . Taking the upper limit for thermal dust emission associated with the central CO concentration estimated in section 3 ( $\leq 3 \text{ mJy}$ ), equation (5) gives an upper limit to the gas mass of  $1.1 \times 10^9 M_{\odot}$ , which is close to the gas mass obtained for the optically thin limit estimate, but at least two times smaller than the other estimates for the CO emission. Table 3 summarizes the various mass determinations.

All of the above mass estimates are intrinsically uncertain by factors of 2 to 3 due to the poorly known millimeter dust emissivities and CO flux to  $\text{H}_2$  column density conversion factors. With the exception of the even more uncertain far-infrared estimates the agreement between the different mass values in Table 3 is thus quite satisfactory. Leaving out the more uncertain mass determined from fitting the far-infrared spectral energy distribution (Draine 1990) the mean of all estimates gives a gas mass of  $\approx 2 \times 10^9 M_{\odot}$  in the central  $R=1''$ . This value is very close to the radiative transport estimate (equation 2) suggesting that the optical depth of the  $1 \rightarrow 0$  and  $2 \rightarrow 1$   $^{12}\text{CO}$  lines is moderate ( $\tau$  of 1 to a few), and significantly smaller than in the average molecular cloud medium in the disk of our own Galaxy, where the typical CO optical depths range from 10 to 30. The difference plausibly lies in the very large local line widths of the highly turbulent gas flows throughout the central kiloparsec of NGC 6240, which is somewhat reminiscent of the broad line molecular cloud features in the center of our Galaxy.

The discrepancy between the best mass estimates from the CO emission and that from the 1.3 mm continuum emission from dust is interesting, especially since the latter is only an upper limit and there is no obvious continuum peak at the CO concentration. It is possible that the dust temperature in the high density core of the gas disk, being relatively far away from the luminous nuclei, is significantly lower than the temperature characterizing the far-infrared emitting dust grains. In fact the Draine (1990) modeling of the overall infrared

to millimeter spectral energy distribution of NGC 6240 suggests that the dust mass may be dominated by cooler, 20–25 K dust. In a situation where cloud-cloud shocks play a very important role, gas and dust temperatures may very well be decoupled. Dust temperatures from the cooler cloud cores may then be significantly lower than the gas temperatures from the shock heated cloud surfaces. In that case the limit inferred from equation (5) would be 2 to 2.6 times greater, in much better agreement with the best estimates from the CO emission.

### 4.3. Mass Modeling

Another means for determining the mass distribution in NGC 6240 can be applied because of the good qualitative agreement between the spatial distributions of dynamical mass and CO flux. Following the method of Scoville et al. (1997) and Tacconi et al. (1999) we treat  $\beta = X/X_G$  in equation (3) as a free parameter and solve for it by finding the best fit of the sum of gas and stellar mass to the spatial distribution of the dynamical mass. This approach exploits the fact that the dynamical mass distribution has a characteristic bump at  $R=0.5 - 1''$  that needs to be matched. It is fairly straightforward to estimate the mass of stars in the young, but aging, starburst of NGC 6240, since this component is well traced by the K-band light. The deep stellar absorption features (CO overtone bands, Mg, Ca, Na etc.) in the K-band require an underlying early M- supergiant stellar population, and imply an age of  $1 - 3 \times 10^7$  years for a short duration burst (Lester et al. 1988, Tezca et al. 1999). The low  $\text{Br}\gamma$  equivalent width and  $[\text{NeIII}]/[\text{NeII}]$  ratio are consistent with this estimate, and also require that the starburst duration be significantly shorter than its age (Tezca et al. 1999). With these constraints and a Scalo (1986) initial mass function between 0.2 and  $100 M_\odot$ , the mass to K-band luminosity ratio is  $\geq 0.5$  (e.g. Thatte et al. 1997). With an effective V-band screen extinction of 5 to 7 mag (or alternatively 40 mag of ‘mixed’

extinction, see Genzel et al. 1998) the mass of young stars in the starburst component is

$$M_*(\text{young}) = 9.3 \times 10^7 \left[ \frac{M_* / L(K)}{0.5} \right] \left[ \frac{\exp(0.09A(V))}{1.9} \right] S(K) \quad [\text{M}_\odot] \quad (6)$$

where  $S(K)$  is the observed K-band flux density in mJy. Within  $R \leq 1''$   $S(K) \sim 13.5$  mJy so that  $M_*(\text{young}) \sim 1.3 \times 10^9 \text{ M}_\odot$  (Tecza et al. 1999).

While this estimate shows that the southern and northern nuclei must be fairly massive entities just based on their young star content, their masses could be larger still if they are the nuclei of the progenitor galaxies with a large additional old stellar component. The mass of the old stellar component cannot be determined from the near- infrared data, however. We can derive an upper limit to the gas mass fraction by simply neglecting the old stellar contribution to the mass. In this case a good fit to the dynamical mass distribution is obtained for  $\beta \sim 0.35$  and  $M_{gas}/M_{dyn} \sim 0.75-0.85$ . Another, perhaps more plausible, approach is to assume that an old stellar component is present and that its radial distribution is similar to that of the young stars. If the underlying old stellar component were similar to that of our own Galaxy the old stellar mass within 500 pc would be  $2.5 - 4 \times 10^9 \text{ M}_\odot$ , so that  $M_*(\text{young+old}) \sim 3-4M_*(\text{young})$ . With this range of old to young stellar mass ratios the best match to the shape of the mass distribution is obtained from the CO rotation curve and second moment map with  $\beta \sim 0.18 - 0.3$  and  $M_{gas}/M_{dyn} \sim 0.4 - 0.7$ . The case of  $\beta=0.25$  is shown in Figure 7. Larger stellar masses and smaller values of  $\beta$  fail to reproduce the relative amplitude of the bump in the dynamical mass model. In contrast smaller stellar masses and larger values of  $\beta$  fit better. For  $\beta=0.25$  the gas mass in the central  $R=1''$  then is  $4 \times 10^9 \text{ M}_\odot$  and  $M_{gas}/M_{dyn} \sim 0.6$ . This mass estimate is listed in the last row of Table 3. **Our mass model suggests that the gas mass fraction is even higher (i.e.  $\sim 1$ ) within  $0''.3$  of the CO peak.**

Solomon et al. (1997) have estimated a dynamical mass from the linewidth of their single dish CO J=1 $\rightarrow$ 0 spectrum. In their work they assume that the CO brightness

temperature is the same as the far-infrared blackbody dust temperature, compare that with the single dish CO luminosity and derive a minimum CO emission radius. Their dynamical mass estimate of  $10^{10} M_{\odot}$  in a  $1''$  radius is nearly a factor of 2 larger than our derived estimate in Table 3. The discrepancy is due to the fact that the Solomon et al. estimate was derived assuming that the entire single dish CO linewidth was due to the circular rotation of the gas within this radius. Given the different assumptions used by Solomon et al. and this work to calculate the dynamical mass within the central  $R=1''$  a factor of 2 agreement seems entirely reasonable.

## 5. Fate of the Central Gas Concentration

In the last section we have shown that a highly turbulent disk of interstellar gas is in the process of settling within the central few hundred parsecs of the merger NGC 6240, and constitutes a considerable fraction (between 30–70%) of the dynamical mass there. This key result of the observations is not expected on the basis of recent N-body simulations of mergers with gas. Barnes and Hernquist (1996) and Mihos and Hernquist (1996) find that the gas component rapidly dissipates angular momentum and forms rotating central disk/bar concentrations on scales  $\leq 1$  kpc around the progenitor nuclei. Such rapidly rotating, cold circum-nuclear disks are, in fact, observed in Arp 220 and several other ULIRGs (Scoville et al. 1997, Downes and Solomon 1998, Sakamoto et al. 1999). However, the simulations do not show cases where the gas becomes self-gravitating and forms a central concentration between the nuclei, as we observe in NGC 6240.

The difference in the molecular spatial distributions and other characteristics between NGC 6240 and several of the other ULIRGs (including Arp 220) may be understandable in terms of NGC 6240 being in an earlier stage of merger evolution than the other studied galaxies. Simulations by Barnes and Hernquist do show that, shortly after the

first encounter of two equal mass, gas-rich galaxies, a significant amount of gas can be ram-pressure stripped from the disks of the progenitors and reside in the interface region between the disks. During this phase no stellar mass is expected in this region, however, and this phase is relatively short-lived as the galaxies fall back toward each other for the next encounter. The projected linear separation of the two nuclei of NGC 6240 (730 pc) is a factor of 2 greater than that of Arp 220 (350 pc). In Arp 220 the true nuclear separation may be  $\sim 1.5$  times the observed one (550 pc; Scoville et al. 1997; Downes and Solomon, 1998). In NGC 6240 the observed differential velocity between the two nuclei seen in both optical and near-infrared spectroscopy is  $\sim 100\text{--}150 \text{ km s}^{-1}$  (Fried and Schulz 1983; Tecza et al. 1999). This indicates that either the true nuclear separation could be much larger than the projected one, between 1.5–3.5 kpc, or that the nuclei are merging on radial, rather than circular orbits. The former conclusion would further strengthen our finding that, in the central  $R=1''$  centered on the CO peak, gas, and not the stars, dominates the mass. Much of the stellar mass included in our mass modelling in section 4.3 may actually be far outside the central region.

The conclusion that NGC 6240 could be in an earlier merging stage than Arp 220 and other ULIRGs is consistent with its having a lower luminosity. The simulations of Mihos and Hernquist (1996) predict that in the merging of disk galaxies with bulges there are several starburst episodes associated with each peri-passage of the two galaxies. The most luminous starburst occurs in the last phase when the two nuclei merge into a single one, and NGC 6240 is likely to be in this final phase given the fact that the two close nuclei will probably not separate again.

### 5.1. Rapid Dissipation of Random Motions

NGC 6240 stands out among luminous infrared galaxies by having the most luminous infrared line emission from hot molecular hydrogen. For a wide range of physical conditions the brightest H<sub>2</sub> infrared line is the v=0-0 S(1) line at 17μm. The dereddened luminosity of that line in NGC 6240 is  $3 \times 10^8 L_{\odot}$  (Egami et al. 1999). ISO and ground-based observations of a number of rotational and ro-vibrational H<sub>2</sub> lines show that the total luminosity in all infrared H<sub>2</sub> lines is at least 7 times greater than that of the 17μm S(1) line (Tecza et al. 1999; Egami et al. 1999), so  $L(H_2) \sim 2 \times 10^9 L_{\odot}$ . This corresponds to 0.3% of the bolometric luminosity of NGC 6240. By comparison, the fractional H<sub>2</sub> luminosity in Arp 220 and a sample of about a dozen other luminous infrared galaxies is between 2 and 10 times smaller (Rigopoulou et al. 1999). Another galaxy with comparable  $L(H_2)/L(FIR)$  is the Antennae (NGC 4038/39) system. In this colliding galaxy system the nuclei have a separation of ~6 kpc, and there is also a prominent concentration of molecular gas in the interaction region between the nuclei (Stanford et al. 1990).

Based on the large  $2\mu\text{m } 1 \rightarrow 0 \text{ S}(1) \text{ H}_2/\text{Br}\gamma$  line ratio, van der Werf et al. (1993) have concluded that the most likely process exciting the H<sub>2</sub> line emission in NGC 6240 is slow ( $\leq 40 \text{ km s}^{-1}$ ) C-shocks in cloud-cloud collisions. This is supported by the H<sub>2</sub> level populations derived from the recent ISO observations of Egami et al. (1999). In such shocks line emission from a number of species other than H<sub>2</sub> (OH, CO, [OI]) is expected to be significant so that  $L(H_2)$  is a lower limit to the total cooling rate.

From the intense H<sub>2</sub> line emission it follows that the large local random velocities must dissipate rapidly. The dissipation time  $\tau_{diss}$  within  $R \leq 470 \text{ pc}$  is then given by

$$\tau_{diss} \leq 1.5 M_{gas} \sigma^2 / L(H_2) \sim 10^{6.8} M_{9.3} \sigma_{130}^2 / L(H_2)_{9.3} \quad [\text{yrs}] \quad (7)$$

where  $\sigma_{130}$  is the average local velocity dispersion in units of  $130 \text{ km s}^{-1}$ ,  $M_{9.5}$  is the gas



mass in units of  $3 \times 10^9 M_\odot$ , and  $L(\text{H}_2)_{9.3}$  is the  $\text{H}_2$  luminosity in units of  $2 \times 10^9 L_\odot$ . The dissipation time scale in the central disk thus is only about 2 to 3 dynamical time scales! We conclude that the present, highly turbulent flow will probably settle to a dynamically cold disk supported largely by rotation in  $< 10^7$  years. This time is significantly shorter than the present orbital time scale of the two nuclei ( $\geq 10^{7.5}$  years) that determines the ‘clock’ of the merger.

## 5.2. Onset of star formation in the central gas disk

One of the surprising results of this study of NGC 6240 is that, despite the very high central  $\text{H}_2$  column densities ( $N(\text{H}_2) \sim 1 - 2 \times 10^{23} \text{ cm}^{-2}$ ,  $\Sigma \sim 10^{3.6} M_\odot \text{ pc}^{-3}$ ) most of the present star forming activity is occurring in the two nuclei as shown by the radio continuum map of Colbert et al. (1994) and the K-band and  $\text{Br}\gamma$  maps of Tecza et al. (1999). However, the basic ‘Toomre criterion’ (1964) for a rotating disk with rotation velocity  $v_{rot}$ , and effective ‘sound speed’  $v_s$  requires that for a disk of surface density  $\Sigma$  to be gravitationally unstable,  $v_s$  must be smaller than

$$v_s \leq \zeta(G\Sigma R/v_{rot}) \sim 11\Sigma_{23}R_{0.5}/v_{250} \quad [\text{km s}^{-1}] \quad (8)$$

where  $\Sigma_{23}$  is the  $\text{H}_2$  column density in units of  $10^{23} \text{ cm}^{-2}$ ,  $v_{250}$  is the rotation velocity in units of  $250 \text{ km s}^{-1}$  and  $\zeta$  is a dimensionless number between 1.1 and 1.6 (see chapter 5.3 in Binney and Tremaine 1987). For  $v_s \sim \sigma \sim 130 \text{ km s}^{-1}$  the disk cannot locally collapse and form stars and the effective Jeans mass is very large (a few  $\times 10^5 M_\odot$ ). Only when the dispersion has dissipated to less than  $10 \text{ km s}^{-1}$  can local gravitational instability set in.

We thus conclude that in a few dynamical time scales ( $\leq 10^7$  years), and perhaps triggered by the next peri-passage of the two nuclei, NGC 6240 may experience a major starburst in the central CO disk and more closely resemble Arp 220 and other ULIRGs.

NGC 6240 and Arp 220, thus, support the scenario (Mihos and Hernquist 1996, Genzel et al. 1998, Genzel, Lutz and Tacconi 1998) that mergers go through several short phases of very active star formation. It remains unclear for NGC 6240 during this process what fraction of the gas mass then will be in the general central gas disk and how much will collect in smaller circumnuclear disks around the progenitor nuclei. In Arp 220 this ratio is about 1:1 (Downes and Solomon 1998; Sakamoto et al. 1999).

## 6. Conclusions

From our high resolution study of the molecular gas in NGC 6240 we have found:

- About half of the CO flux is concentrated in a thick disk-like structure located between the IR/radio nuclei. The velocity structure of this disk is highly disturbed, with unusually large line widths of FWZP 700–1000 km s<sup>-1</sup> almost everywhere within the central 3'' from the CO peak.
- Modeling of the data shows that the gas is rotationally supported, but with a very large local velocity dispersion characteristic of a hot dynamical system. The inferred average ratio of rotational velocity in the central disk to local one dimensional velocity dispersion is  $\langle v_{rot} \rangle / \sigma \sim 2$  with a range of 1 to 3. This indicates that the disk is highly turbulent and geometrically thick.
- Based on several methods to estimate the gas mass and mass models for NGC 6240 we find that the mass of the gas disk within the central  $R \leq 1''$  is  $2 - 4 \times 10^9 M_{\odot}$ , and constitutes between 30% and 70% of the dynamical mass in this region. Self-gravitating gas concentrations thus may play a significant role in the evolution of mergers.

- NGC 6240 is likely in an earlier merger stage than typical ULIRGs. From the very high luminosity in the infrared H<sub>2</sub> lines we conclude that the local random velocities will dissipate in a few dynamical times ( $< 10^7$  years). Once this happens, NGC 6240 will form a dense, geometrically thin central gas disk and will be ripe for a major starburst. With its luminosity then rising and its ISM more confined, it could then more closely resemble Arp 220 and other ULIRGs.

Acknowledgements. We thank the staff of IRAM for their help with carrying out the observations and calibrations. We are grateful to E.Colbert for providing us with a FITS image of his 8 GHz radio map. We also thank R.Bender for interesting discussions, and the referee, Chris Mihos, for many useful suggestions which helped to improve the final version of this paper.

## REFERENCES

- Armus, L., Heckman, T.M. and Miley, G.K. 1990, *ApJ*, 364, 471
- Barnes, J.E., and Hernquist, L. 1996, *ApJ*, 471, 115
- Bender, R., Saglia, R.P. and Gerhard, O.E. 1994, *MNRAS*, 269, 785
- Binney, J. and Tremaine, S. 1987, *Galactic Dynamics* Princeton: Princeton University Press
- Bland-Hawthorn, J., Wilson, A.S. and Tully, R.B. 1991, *ApJ*, 371, L19
- Bloemen, H. 1989, *ARA&A*, 27, 469
- Bryant, P.M. and Scoville, N.Z. 1996, *ApJ*, 457, 678
- Bryant, P.M. and Scoville, N.Z. 1999, *AJ*, submitted
- Casoli, F., Dupraz, C. and Combes, F. 1992, *A&A*, 264, 55
- Colbert, E.J.M., Wilson, A.S. and Bland-Hawthorn, J. 1994, *ApJ*, 436, 89
- Combes, F., Casoli, F., Encrenaz, P., Gerin, M., and Laurent, C. 1991, *A&A*, 248, 607
- Dickman, R.L., Snell, R. and Schloerb, F.P. 1986, *ApJ*, 309, 326
- Downes, D., Solomon, P.M. and Radford, S.J.E. 1993, *ApJ*, 414, L13
- Downes, D. and Solomon, P.M. 1998, *ApJ*, 507,615
- Doyon, R., Wells, M., Wright, G.S., Joseph, R.D., Nadeau, D. and James, P.A. 1994, *ApJ*, 437, L23
- Draine, B.T. and Lee, H.M. 1984, *ApJ*, 285, 89
- Draine, B.T. 1990, *The Interstellar Medium in Galaxies*, H.A.Thronson and J.M. Shull, Dordrecht:Kluwer, 483
- Dutrey, A., Guilloteau, S. and Simon, M. 1994, *A&A*, 286, 149
- Egami, E. et al. 1999, in preparation

- Fried, J.W. and Schulz, H. 1983, *A&A*, 118, 166
- Genzel, R. 1992, *The Galactic Interstellar Medium*, D. Pfenninger and P. Bartholdi, Berlin:Springer, 275
- Genzel, R. et al. 1998, *ApJ*, 498, 579
- Genzel, R., Lutz, D. and Tacconi, L.J. 1998, *Nature*, 395, 859
- Guilloteau, S. et al. 1992, *A&A*, 262, 624
- Heckman, T.M., Armus, L. and Miley, G.K. 1987, *AJ*, 92, 276
- Heckman, T.M., Armus, L. and Miley, G.K. 1990, *ApJS*, 74, 833
- Herbst, T.M., Graham, J.R., Tsutsui, K., Beckwith, S., Matthews, K., and Soifer, B.T. 1990, *AJ*, 99, 1773
- Joseph, R.D., Wright, G.S. and Wade, R. 1984, *Nature*, 311, 132
- Kii, T., Nakagawa, T., Fujimoto, R. Ogasaka, T., Miyazaki, T., Kawabe, R. and Terashima, Y. 1997, *X-Ray Imaging and Spectroscopy of Cosmic Hot Plasmas*, F.Makino and K.Mitsuda, Tokyo:Universal Academy Press, 161
- Lester, D.F., Harvey, P.M. and Carr, J. 1988, *ApJ*, 329, 641
- Lester, D.F. and Gaffney, N.J. 1994, *ApJ*, 431, L13
- Lutz, D. et al. 1996, *A&A*, 315, L137
- Mihos, J.C. and Hernquist, L. 1996, *ApJ*, 464, 641
- Nakagawa, T. et al. 1999, in preparation
- Rigopoulou, D. et al. 1999, in preparation
- Sakamoto, K., Scoville, N.Z., Yun, M.S., Crozas. M., Genzel, R. and Tacconi, L.J. 1999, *ApJ*, March 1

- Sanders, D.B., Soifer, B.T., Elias, J.H., Madore, B.F., Matthews, K., Neugebauer, G. and Scoville, N.Z. 1988, *ApJ*, 325, 74
- Sanders, D.B. and Mirabel, I.F. 1996, *ARA&A*, 34, 749
- Scalo, J. 1986, *Fundamentals of Cosmic Physics*, 11, 1
- Scoville, N.Z., Yun, M.S. and Bryant, P.M. 1997, *ApJ*, 484, 702
- Solomon, P.M., Downes, D., Radford, S.J.E. and Barrett, J.W. 1997, *ApJ*, 478, 144
- Stanford, S.A., Sargent, A.I., Sanders, D.B., and Scoville, N.Z. 1990, *ApJ*, 349, 492
- Tacconi, L.J., Genzel, R., Blietz, M., Cameron, M., Harris, A.I. and Madden, S. 1994, *ApJ*, 426, L77
- Tacconi, L.J. et al. 1999, in preparation
- Tecza, M., et al. 1999, in preparation
- Thatte, N., Quirrenbach, A., Genzel, R., Maiolino, R. and Tecza, M. 1997, *ApJ*, 490, 238
- Thronson, H.A., Majewski, S., Descartes, L. and Hereld, M. 1990, *ApJ*, 364, 456
- Toomre, A. 1964, *ApJ*, 139, 1217
- Van der Werf, P.P., Genzel, R., Krabbe, A., Blietz, M., Lutz, D., Drapatz, S., Ward, M. and Forbes, D.A. 1993, *ApJ*, 405, 522
- Wang, Z., Scoville, N.Z. and Sanders, D.B. 1991, *ApJ*, 368, 112
- Whitmore, B.C., McElroy, D.B. and Tonry, J.L. 1985, *ApJS*, 59, 1
- Wilkinson, P.N. 1992, in *Subarcsecond Radio Astronomy*, R. J. Davis & R. S. Booth, eds. [Cambridge University Press: Cambridge], 422
- Yun, M.S. and Scoville, N.Z. 1995, *ApJ*, 451, L45

Fig. 1.— Selected CO J=2→1 line spectra (20 km s<sup>-1</sup> resolution) superposed on a false color image of the integrated CO 2→1 flux distribution (logarithmic stretch). The slightly overresolved synthesized beam with 0′.5 × 0′.7 FWHM resolution is shown as a red ellipse in the lower left. Letters A through E mark the gas features discussed in section 3 of the text. The two asterisks mark the positions of the south and north radio/infrared nuclei, and the crosses mark the positions of the spectra.

Fig. 2.— Uniformly weighted velocity channel maps of the CO J=2→1 emission in steps of 40 km s<sup>-1</sup> and with a spatial resolution of 0′.5 × 0′.9 FWHM. The cross denotes the position of the CO flux peak. Contours run from -18 to -6 mJy beam<sup>-1</sup> and from 6 to 36 mJy beam<sup>-1</sup> in steps of 6 mJy beam<sup>-1</sup> ( $\sim 3\sigma$  per 40 km s<sup>-1</sup> channel).

Fig. 3.— Left: 1.315mm (228 GHz) continuum map at 0′.5 × 0′.9 FWHM resolution. Contours start at 0.7 mJy beam<sup>-1</sup> ( $\sim 3\sigma$ ) and increase in steps of 0.7 mJy beam<sup>-1</sup>. The cross denotes the position of the CO flux peak. Right: Redshifted CO emission (intensity weighted sum from 345 to 545 km s<sup>-1</sup>, thin contours) and blueshifted CO emission (intensity weighted sum from -535 to -335 km s<sup>-1</sup>, heavy contours). Contours run in steps of 10% of the peak in each case. The cross denotes the position of the CO flux peak.

Fig. 4.— Top: Contour and grey scale map of the CO 2→1 velocity dispersion. Contours run from  $\sigma_{moment}=60$  to 200 km s<sup>-1</sup> in steps of 20 km s<sup>-1</sup>. Middle: Position- velocity map of the CO 2→1 emission along the direction of largest velocity gradient (P.A.=40°) in the central disk. Bottom: Position -velocity map of the best fitting axisymmetric rotating disk model (thin contours, Table 2) superposed on the data (heavy contours).

Fig. 5.— Overlay of model profiles of rotating disk (thin line; parameters as in Table 2) on CO 2→1 spectra (thick lines), for selected positions in the central CO disk. Data and model are at a resolution of 0′.5 × 0′.9 resolution. Velocities are relative to 7389 km s<sup>-1</sup>. Position

offsets from the CO peak are given in parentheses in the top left of each box.

Fig. 6.— Top: Overlay of a logarithmically spaced contour map of the 8 GHz radio continuum emission (resolution  $0''.15$  FWHM, Colbert et al. 1994) on a false color map of the CO 2→1 integrated flux (logarithmic stretch). Radio contours run from  $10^{-1}$  to  $10^{1.2}$  mJy in steps of  $10^{0.2}$ . Middle: Overlay of a logarithmically spaced contour map of the 5 GHz MERLIN radio continuum emission (resolution  $94 \times 50$  milliarcsec at P.A.  $21^\circ$ ) on the false color linear scale CO map to emphasize the central gas disk and the compactness of the radio nuclei. Bottom: Logarithmic false color 8 GHz radio continuum map (as before, Colbert et al. 1994) with redshifted (intensity weighted sum from 345 to 545  $\text{km s}^{-1}$ , thin red contours) and blueshifted (intensity weighted sum from  $-535$  to  $-335$   $\text{km s}^{-1}$ , heavy light blue contours) CO 2→1 emission contours superposed. The cross denotes the position of the CO flux 2→1 peak.

Fig. 7.— Left: CO model rotation curve (Table 2) shown as a heavy curve; CO 2→1 second moment map (CO dispersion  $\sigma_{moment}$ ) converted to circular velocity, ( $v_{circ}(\text{CO}) \sim \sqrt{2}\sigma_{moment}$ , see footnote 5), plotted as crosses and connected by thin lines; and the square root of the observed CO flux distribution divided by radius in dashed lines scaled to match. Right: Mass models in the central  $1''.4$  (see text). The light solid curve shows the stellar mass for the case  $M_{old} + M_{young} \approx 3 \times M_{young}$ ; the medium solid curve is the distribution of  $M_{gas}$  assuming the CO-to- $\text{H}_2$  conversion factor is 0.2 times the Galactic value of Bloemen et al. (1989); the dashed line shows the model dynamical mass distribution; the filled squares represent dynamical mass distribution derived from the CO moment map; and the heavy solid curve shows the total of the observed gas and stellar mass. For this case  $M_{gas}/M_{dyn} \approx 0.5$ . Better fits to the characteristic shape of the dynamical mass distribution can be achieved with larger  $M_{gas}/M_{dyn}$  ratios and correspondingly smaller contributions of old stars in the central  $R \leq 1''$ .



Table 1. Basic Observational Parameters

---

---

Total CO 2→1 flux	1220 Jy km s <sup>-1</sup>
CO 2→1 flux in central R=1''	528 Jy km s <sup>-1</sup>
Peak CO 2-1 T <sub>b</sub>	21 K
228 GHz cont. flux - south nucleus	4.7 mJy
228 GHz cont. flux - north nucleus	1 mJy

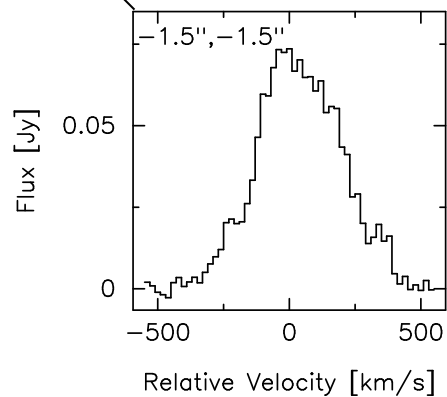
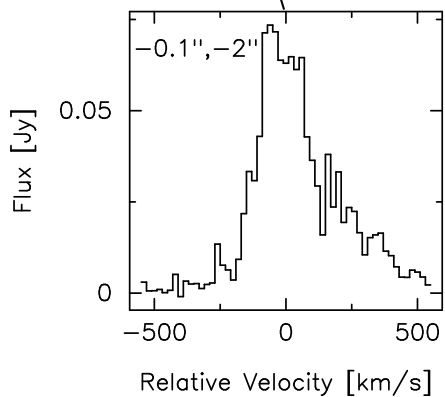
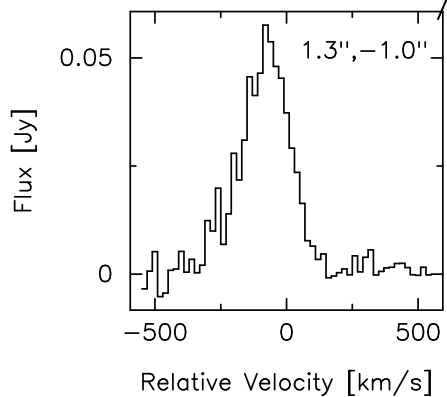
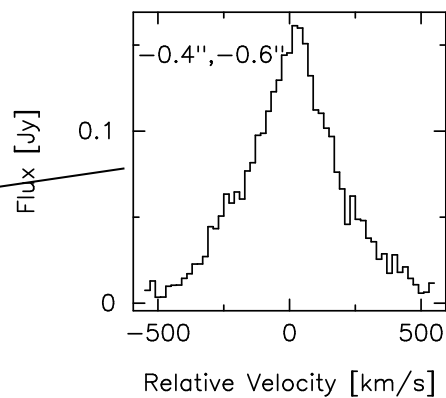
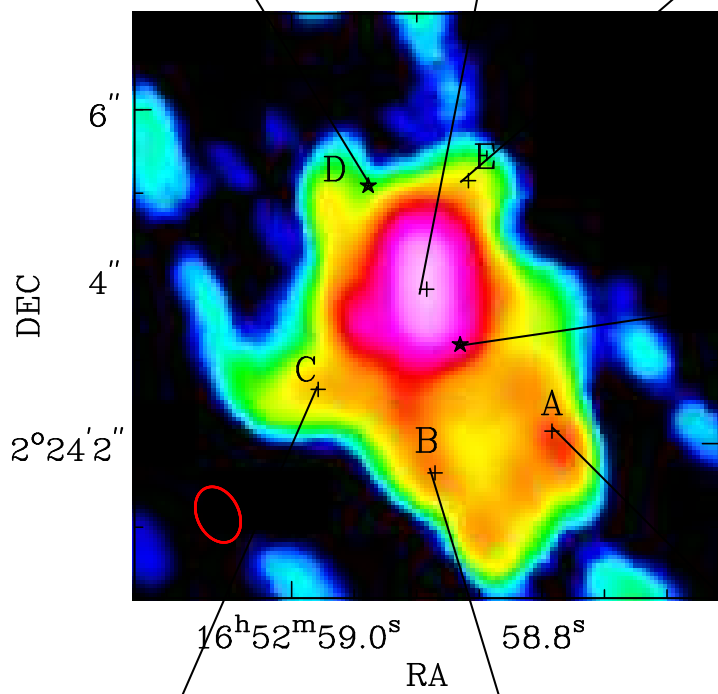
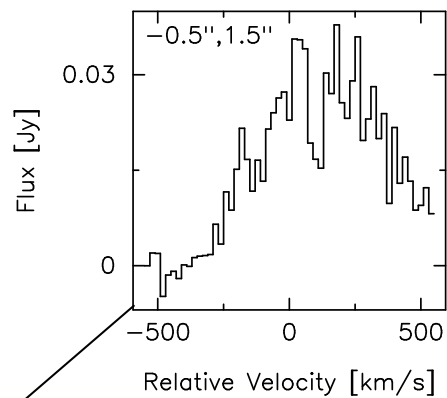
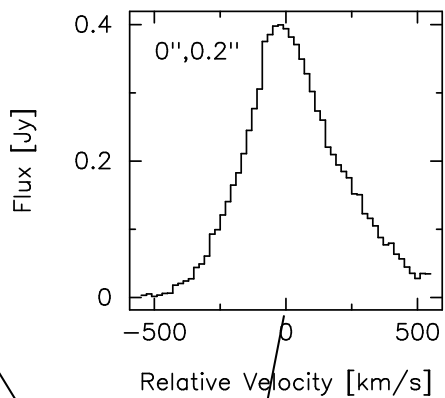
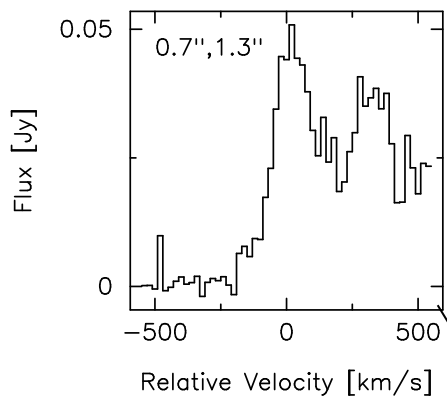
---

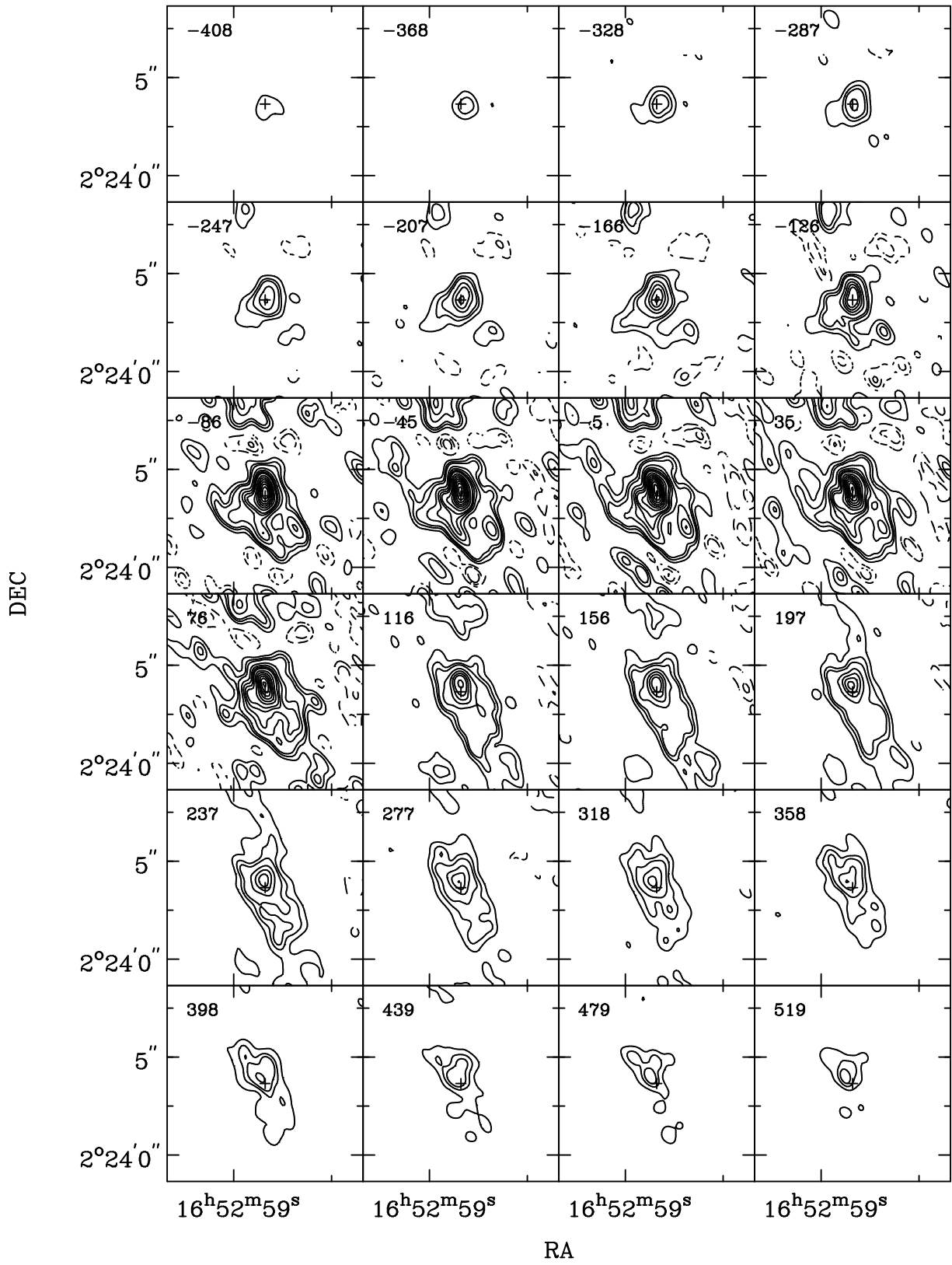
Table 2. Best Fitting Parameters of Axisymmetric Disk Model

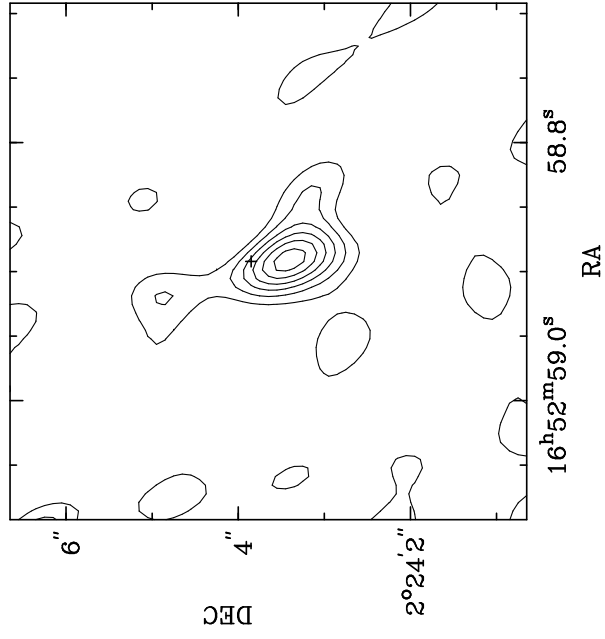
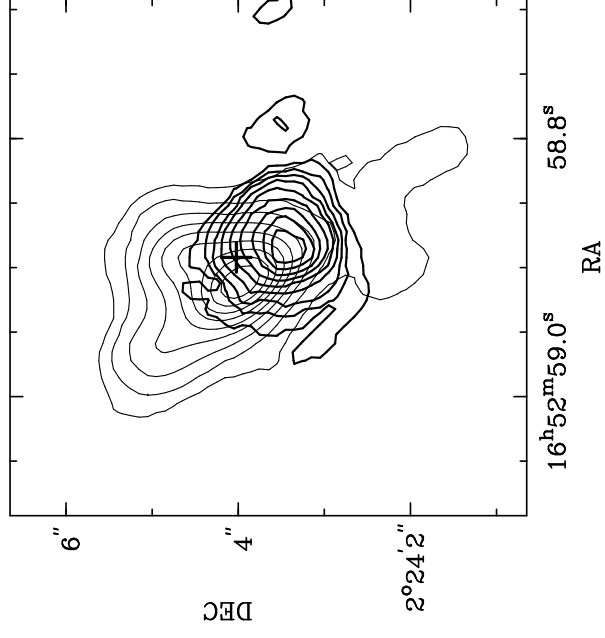
R (arcsec)	$v_{rot}$ (km s <sup>-1</sup> )
0.2	120
0.3	180
0.5	280(±40)
0.75	280
1.0	250
Density distribution	$n(R)=\exp[-2.77((R - 0.1)/0.55)^2]$ $+0.25 \times \exp(-2.77(R/1.5)^2)$ (between 0.01'' and 2'')
Local velocity dispersion	$\sigma=128$ km s <sup>-1</sup>
FWHM z-thickness of disk	0''.7

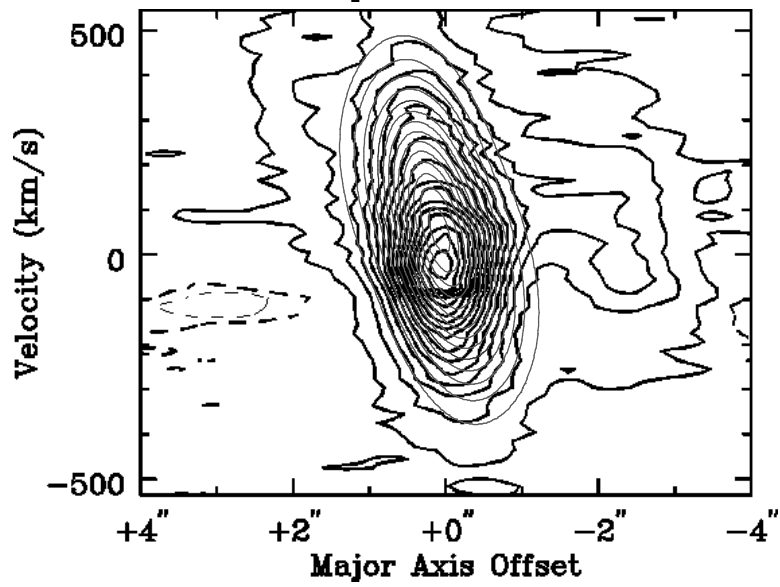
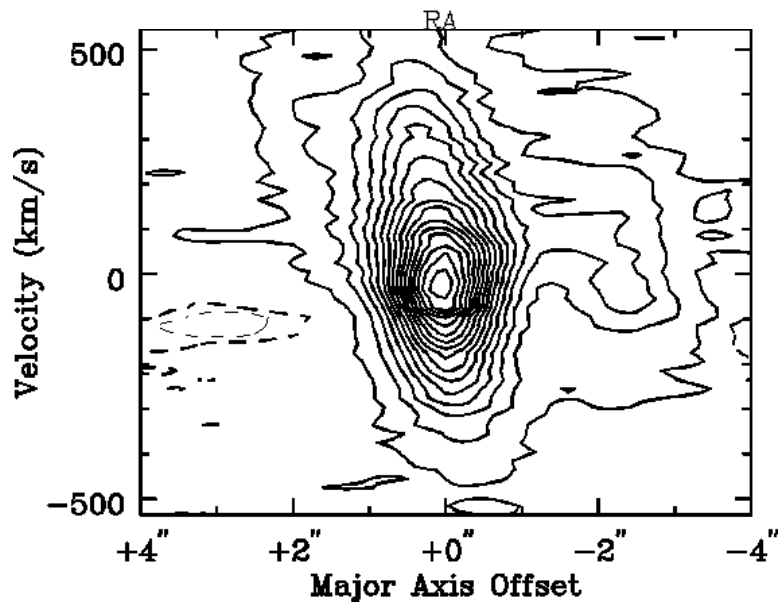
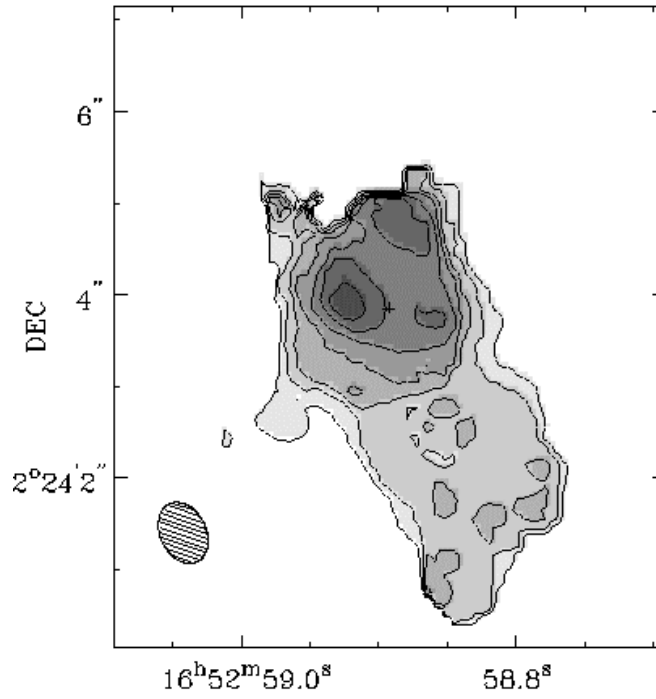
Table 3. Gas Mass Estimates for the Central CO Concentration

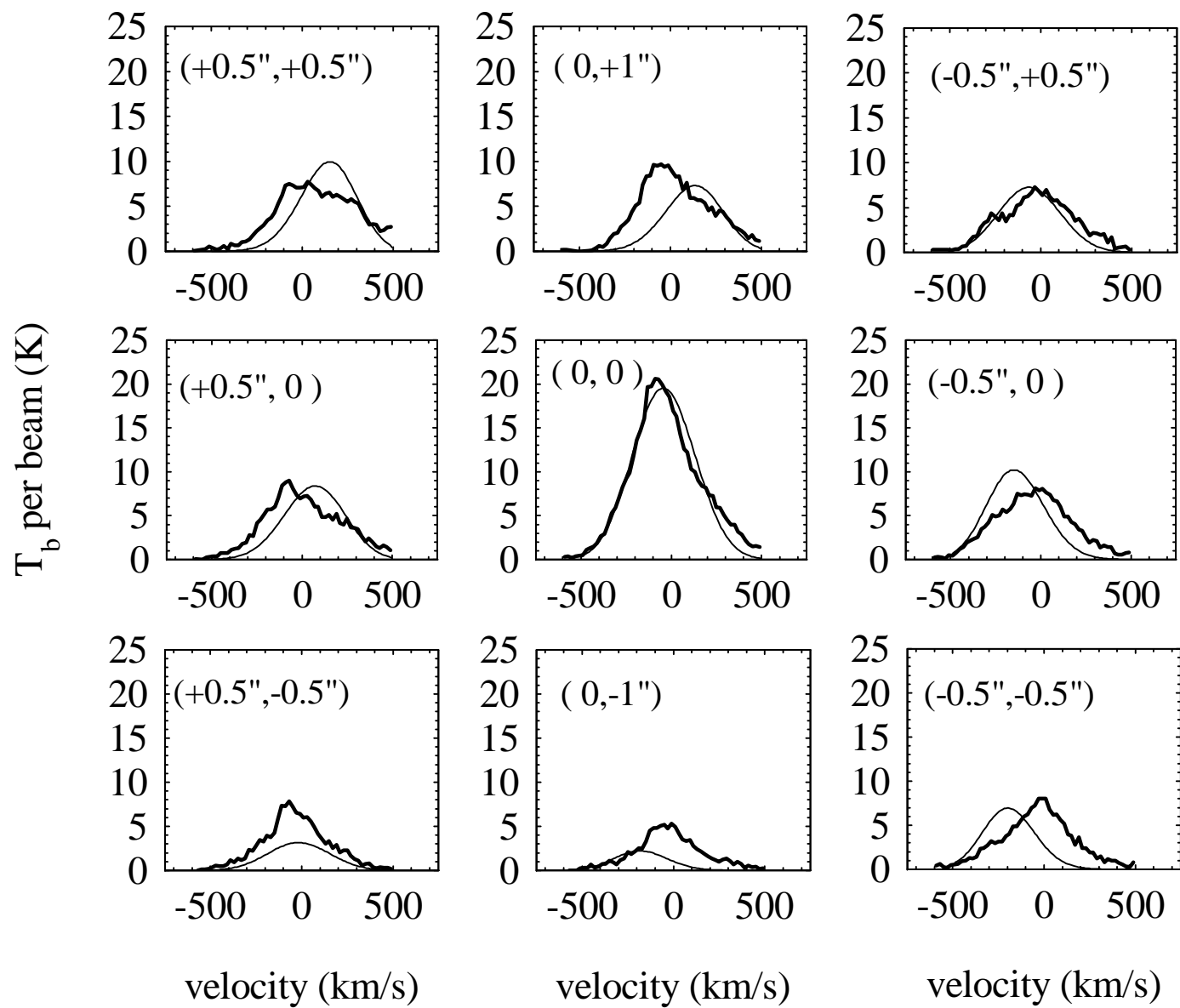
Mass Estimate	Gas Mass Within R=1" (470 pc)
Optically thin CO emission	$1.1 \times 10^9 M_{\odot}$
Radiative transport solution matching $^{12}\text{CO}$ 2→1, 1→0 and $^{13}\text{CO}$ 1→0 lines	$2.2 \times 10^9 M_{\odot}$
Optically thick CO emission	$3 \times 10^9 M_{\odot}$
Far-infrared dust emission	$10(+25, -7) \times 10^9 M_{\odot}$
1.3mm dust emission	$\leq 1.1 \times 10^9(52/T_{dust}) M_{\odot}$
Mass modeling of CO emission	$4 \pm 1 \times 10^9 M_{\odot}$
Dynamical mass	$6.4 \pm 1 \times 10^9 M_{\odot}$



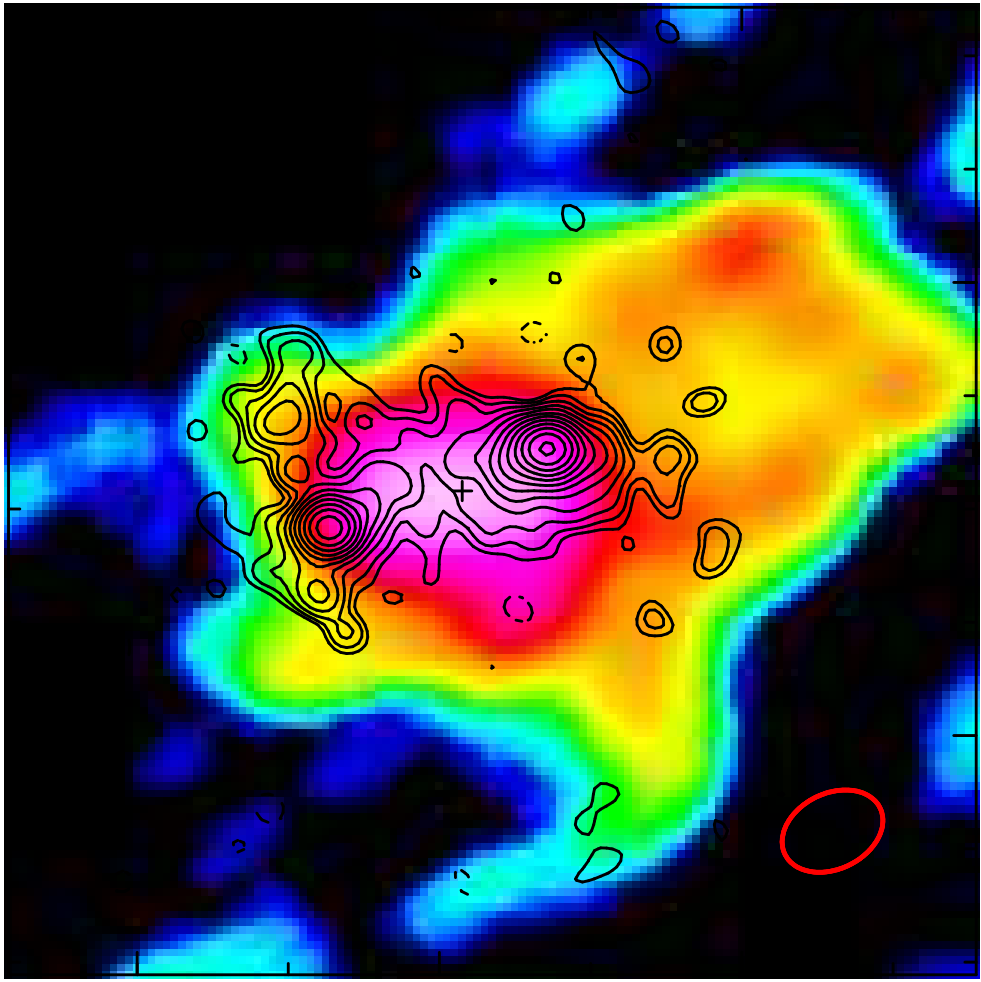












$16^{\text{h}}52^{\text{m}}59.0^{\text{s}}$   $58.8^{\text{s}}$

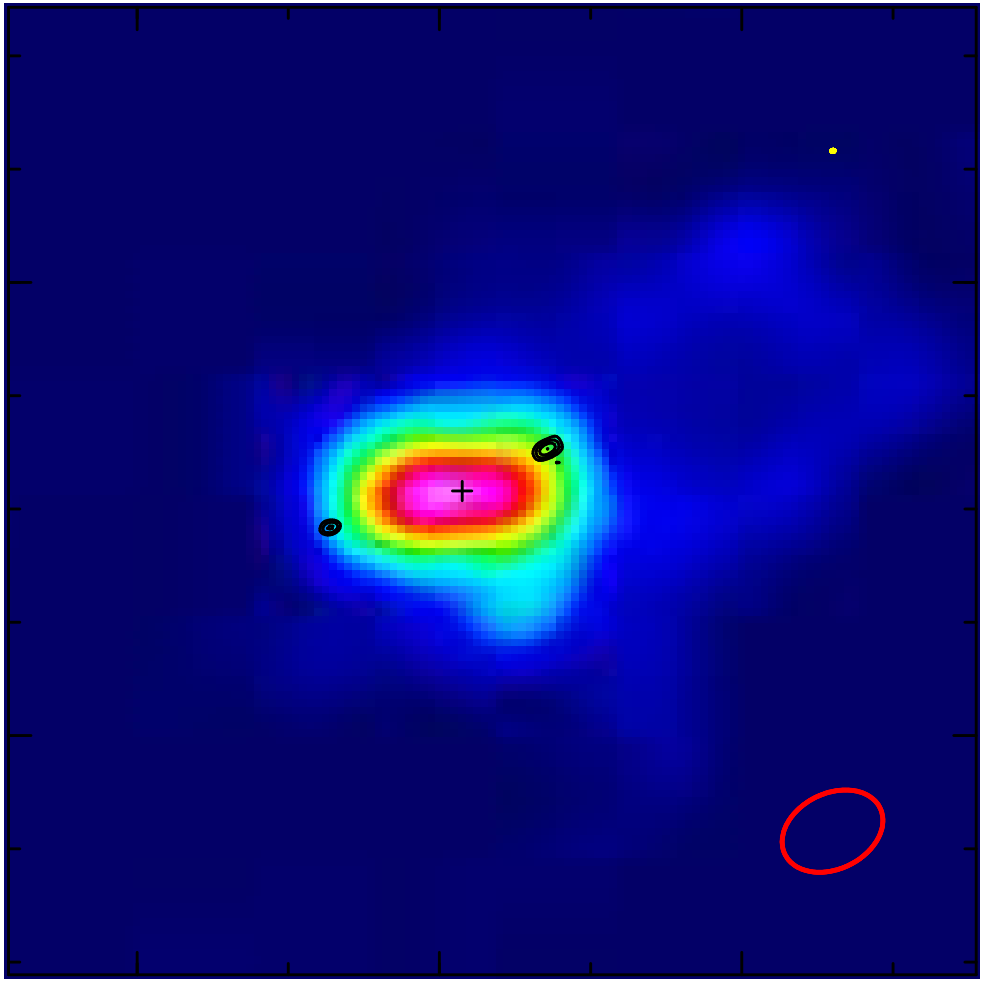
RA

$6''$

$4''$

$2^{\circ}24'2''$

DEC



6"

4"

2°24'2"

DEC

16<sup>h</sup>52<sup>m</sup>59.0<sup>s</sup>

RA

58.8<sup>s</sup>

